The Permeability of Screen Wicks*

Hiroaki KOZAI**, Hideaki IMURA***
and Yuji IKEDA****

An experimental study was performed on the permeability of screen wicks using water. An equation for the wick porosity influencing the permeability was also proposed based on a model of the screen geometry. In the present experiment, the screen mesh size, number of screen layers, packing condition of the screen and flow rate were varied. For the friction factor, a correlation $C_f = A/Re$ was obtained ; here the coefficient A was related to the packing number ω defined by the ratio of n-layer thickness to n-times the single-layer thickness of the screen. Consequently, it was found that the permeability of the screen wicks could be predicted considerably well from the expression presented in this study and increased steeply with the increase in the packing number ω, which showed the degree of hold-down pressure for the screen wicks.

Key Words: Heat Pipe, Porous Media, Permeability, Porosity, Pressure Drop, Screen Wick, Packing Number, Crimping Factor

1. Introduction

The heat pipe can transport a large amount of heat with small temperature difference since it transports heat by utilizing latent heat. However, because the capillary pressure in a wick is used for the return of liquid from the condenser to the evaporator, the working fluid cannot circulate when the pressure drops in the liquid and vapor flows exceed the limit of the capillary pressure. As a result, the heat transfer rate in the heat pipe is restricted. In the design of heat pipe, therefore, it is important to predict the maximum heat transfer rate due to this capillary limitation. For that, the effective pore radius and the permeability of wicks, which determine the limit of the capillary pressure and the pressure drop in the liquid flow through the wick respectively, should be estimated accurately. Therefore, the authors[1] first performed the study on the effective pore radius of screen wicks. From a model of the screen geometry, which was proposed on the basis of the microscopic observation, an equation for the effective pore radius of screen wicks was derived, and its validity was confirmed by the experimental data.

On the other hand, many investigations of the permeability for screen wicks have been carried out. However, the experimental data have been given[2),(3)] for only the individual wicks, and no generally valid correlation has been obtained so far. For the permeability of screen wicks, there is the modified Blake-Kozeny equation[4)~(6)] in which Marcus's equation is used for porosity. However, in Marcus's equation, the influence of the hold-down pressure for the screen wicks is not taken into consideration. Ikeda[7] obtained an equation for the permeability from the analysis based on a screen geometric model and from the experiment in which the number of screen layers was varied from 1 to 3, and the authors[8] also presented an equation from the unsteady flow experiment. However, in these studies, the discussion on the influence of the hold-down pressure for screen wicks

* Received 30th October, 1990. Paper No.89-0878B
** Faculty of Engineering, Kyushu Tokai University, 223 Toroku Ohe-machi, Kumamoto 862, Japan
*** Faculty of Engineering, Kumamoto University, 2-39-1 Kurokami, Kumamoto 860, Japan
**** Kyocera, Ltd., 1810 Taki-cho, Sendai 895-02, Japan

is not made sufficiently.

In the present research, an equation for the porosity of screen wicks is proposed on the basis of the screen geometric model given in the previous report[1]. The experiments are performed on the pressure drop in screen wicks to examine the effects of screen mesh size, number of screen layers and hold-down pressure of the screen, and an expression for the permeability of screen wicks is presented.

2. Nomenclature

A : coefficient in Eq.(19)
A_w : cross-sectional area of channel m^2
b : width of channel m
C_f : friction factor
c : clearance $=\delta_1-2d$ m
d : diameter of screen wire m
d_h : hydraulic diameter m
K : wick permeability m^2
l : length of channel m
M_s : mass of wires in single-layer screen sample kg
$\dot{m}$: mass flow rate kg/s
N : number of screen-wire openings per unit length $=1/(w+d)$ 1/m
n : piled number of screen layers
ΔP : pressure drop Pa
R : radius of curvature of screen wire m
Re : Reynolds number
S : crimping factor of screen
u : average fluid velocity $=u_f/\varepsilon$ m/s
u_f : superficial average fluid velocity $=\dot{m}/(\rho_l A_w)$ m/s
V : volume of wick m^3
V_s : volume of wires in single-layer screen sample m^3
w : screen-wire opening m
Z : coefficient in Eq.(15) [Eq.(16)]
α : dimensionless gap of screen $=c/(2d)$
β : ratio of width and thickness of screen $=b/\delta_1$
δ : thickness of screen m
ε : wick porosity
ν_l : kinematic viscosity of liquid m^2/s
ρ_l, ρ_s : densities of liquid and screen wire kg/m^3
ϕ : angle shown in Fig. 1 rad
ω : packing number $=\delta_n/(n\delta_1)$

Subscripts

m : mean
s : shoot wire
w : warp wire
1, n : 1- and n-layer

3. Screen Geometry

In the previous report[1], a model of the screen geometry shown in Fig. 1 was proposed on the basis of the microscopic observation. From this model, where the shape of the wires in plain square weave screens was approximated by arcs, the porosity ε_1 for single-layer screens is estimated from the equation derived as follows. When the radii of curvature of the warp and shoot wires corresponding to longitudinal and lateral threads of the screen are designated as R_w and R_s, respectively, the following equations hold true :

$$R_w-R_w\cos\phi_w=(d+c)/2 \quad (1)$$
$$R_s-R_s\cos\phi_s=(d-c)/2 \quad (2)$$
$$R_w\sin\phi_w=(w+d)/2 \quad (3)$$
$$R_s\sin\phi_s=(w+d)/2. \quad (4)$$

The combinations of Eqs.(1)~(4) yield the following expressions for R_w, R_s, ϕ_w and ϕ_s :

$$R_w=(w+d)/(2\sin\phi_w) \quad (5)$$
$$R_s=(w+d)/(2\sin\phi_s) \quad (6)$$
$$\phi_w=2\tan^{-1}\{(d+c)/(w+d)\} \quad (7)$$
$$\phi_s=2\tan^{-1}\{(d-c)/(w+d)\}. \quad (8)$$

Therefore, the crimping factors S_w and S_s for the warp and shoot wires are expressed as follows :

$$S_w=2R_w\phi_w/(w+d) \quad (9)$$
$$S_s=2R_s\phi_s/(w+d). \quad (10)$$

Consequently, the porosity for the single-layer screens is expressed by the following equation :

$$\varepsilon_1=1-\pi dS_mN/\{4(1+\alpha)\}, \quad (11)$$

where the mean crimping factor of screens is $S_m=(S_w+S_s)/2$, the mesh number per unit length $N=1/(w+d)$ and the dimensionless gap of the single-layer screen $\alpha=c/(2d)$.

In order to confirm the validity of Eq.(11), the values of ε_1 from Eq.(11) were compared with those of ε_1 computed from Eq.(12):

$$\varepsilon_1=1-V_s/V=1-M_s/(\rho_sV), \quad (12)$$

where the wire volume V_s and the wire mass M_s of the single-layer screen were measured experimentally. The geometric properties of the stainless steel and phosphor bronze plain square weave screens used to estimate the porosity are given in Table 1. A universal measuring microscope was employed for the measure-

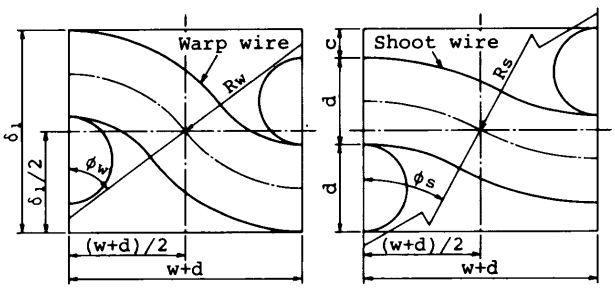

Fig. 1 Model of screen geometry

ment of the screen wire diameter d and opening w, and a micrometer for the single-layer screen thickness δ_1. The volume of the screen wires V_s was obtained from that of ethyl alcohol displaced by immersion of the sample in a measuring cylinder. On the other hand, the mass of the screen wires M_s was measured by an electronic balance. Table 2 shows the comparison of the calculated values from Eq.(11) with the experimental data for the porosity of the single-layer screens. In Table 2, the calculated values ε_1(Cal.) are in close agreement with the experimental ones ε_1(Exp.) within an error of ± 3 % . From this result, it is thought that the porosities ε_1 for the single-layer screens can be predicted well from Eq. (11).

4. Experimental Apparatus and Procedure

The schematic diagram of the apparatus for the measurement of friction factor is shown in Fig. 2. A tank ② and an overflow tank ④ were installed over the test section ①, and in order to prevent the dirt from adhering to the screen samples, filters ③ were fitted at the exits of these two tanks. Figure 3 shows the details of the test section. The flow channel in the test section was constructed of the side walls and the upper and lower holders, which were made of a transparent acrylic resin plate so as to enable observation of the screen samples. In order to seal air leakage into the flow channel, the rubber gasket of 2 mm in thickness and 5 mm in width was bonded to the side walls of the upper holder. The channel height was adjusted by screws. The flow channel of 300 mm in length and 30 mm in width was set horizontally, and the screen samples of 280 mm length were positioned in the middle of the channel. The lower holder has seven pressure taps with a 0.8 mm diameter hole which are indicated by symbols P 1～P 7 in Fig. 3. Five of them P 1～P 5 were located at 50 mm intervals in the longitudinal (flow) direction, and the other two pressure taps P 6 and P 7 on both lateral sides of P 3.

Distilled water was used as the test liquid, and 48, 70, 100 and 200 mesh stainless steel plain square weave screens shown in Table 1 were used as the screen samples. The installed screen thickness was evaluated by subtracting the thickness of the upper and lower plates from the entire thickness of the holders. Pressure drops ΔP were measured with the glass tube water manometers ⑤ shown in Fig. 2. The pressures at the three pressure taps P 3, P 6 and P 7 were almost the same. However, since there were some data on which the influence of the entrance and exit of the channel appeared at the pressure taps P 1 and/or P 5, the value over the middle 100 mm length, i.e., the

Table 1 Geometric properties of screens

Material	Mesh	Wire spacing w [μm]	Wire diameter d [μm]	Thickness δ_1 [μm]	Crimping factor Sw	Crimping factor Ss
Stainless steel	48	308.6	215.8	453	1.13	1.09
	60	257.3	166.1	341	1.11	1.09
	70	209.7	151.3	322	1.14	1.09
	100	149.5	103.0	217	1.13	1.09
	150	112.2	55.5	121	1.10	1.05
	200	78.7	49.7	121	1.19	1.03
	270	62.1	31.0	70	1.11	1.04
Phosphor bronze	50	302.0	205.7	431	1.13	1.09
	60	256.2	168.1	337	1.10	1.10
	70	208.0	150.3	331	1.16	1.07
	100	154.9	103.3	218	1.13	1.08
	140	108.0	72.8	173	1.19	1.04
	200	77.2	50.0	120	1.19	1.04
	250	63.2	37.3	94	1.20	1.02

Table 2 Comparison between calculated and experimental values of porosity for single-layer screens

Material	Mesh	Experiment ε_1(Exp.) Volume	Experiment ε_1(Exp.) Mass	Calculation ε_1(Cal.)
Stainless steel	48	0.664	0.663	0.658
	60	0.678	0.674	0.669
	70	0.665	0.662	0.655
	100	0.666	0.667	0.663
	150	0.732	0.732	0.744
	200	0.711	0.709	0.721
	270	0.723	0.721	0.750
Phosphor bronze	50	0.677	0.682	0.664
	60	0.668	0.673	0.658
	70	0.672	0.677	0.665
	100	0.673	0.677	0.671
	140	0.698	0.696	0.702
	200	0.699	0.698	0.713
	250	0.717	0.728	0.742

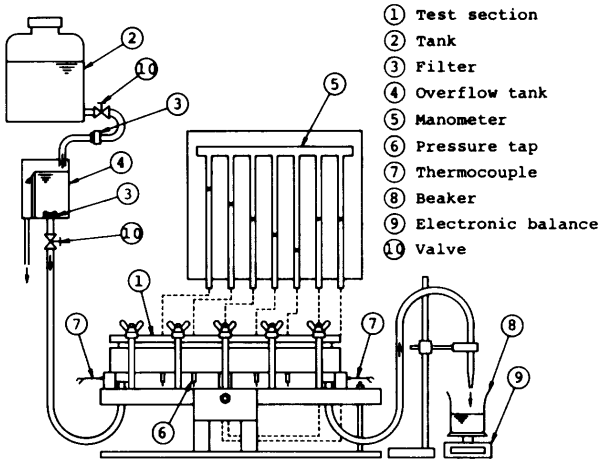

Fig. 2 Schematic diagram of apparatus for measurement of friction factor

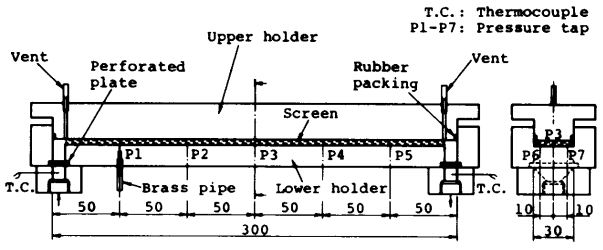

Fig. 3 Details of test section

pressure difference between P2 and P4 was adopted as ΔP. The flow rate was estimated from the mass of the distilled water flowing into a beaker ⑧ during a given time, which was measured with an electronic balance ⑨. The experiment was performed in the following manner. The valve ⑩ fitted at the exit of an overflow tank ④ was opened, and the flow rate was set at a predetermined value. When the liquid levels in the manometers reached a steady state, the flow rate and the pressures at each measuring point were recorded, and the liquid temperatures were measured with the copper-constantan sheathed thermocouples ⑦ fixed at the entrance and exit of the test section. These procedures were repeated with a stepwise increase in the flow rate. In the installation of screens and the measurement of the friction factor, great care was taken to prevent air bubbles from remaining in the screen samples.

5. Experimental Results and Discussion

Figure 4 shows the influence of the packing number ω on the relation between the pressure drop per unit length $\Delta P/l$ and the superficial average fluid velocity u_f. The packing number $\omega=\delta_n/(n\delta_1)$ shows the degree of hold-down pressure for screen wicks. In this figure, the screen sample is indicated in the order of (mesh number)(material)-(number of layers), where the mark S in the second set of parentheses represents the stainless steel screen. In Figs. 4~12, symbols of Warp or W and of Shoot or S represent the flows in the direction of warp and shoot wires, respectively. As seen from Fig. 4, the pressure drops decrease with the increase in the packing number ω. Also, because the experimental data nearly fall on a straight line for each ω, $\Delta P/l$ is linearly proportional to u_f. The influence of the piled number of screen layers n on the pressure drops for the 48 mesh stainless steel screens is shown in Fig. 5. In the case of the same packing number ω, the pressure drops decrease with increasing n, and $\Delta P/l$ is proportional to u_f for each piled number of screen layers.

Before the experimental data are correlated in the relation between the friction factor C_f and the Reynolds number Re, the porosity ε for multilayer screens and the hydraulic diameter d_h pertinent to these two quantities C_f and Re must be described. In the previous report[8], the porosities ε for multilayer screens were estimated from the following equation using the experimental values of the porosity ε_1 for single-layer screens :

$$\varepsilon=1-n\delta_1(1-\varepsilon_1)/\delta_n. \quad (13)$$

However, since it was found that the values of ε_1 can be predicted by Eq.(11), the porosities ε for multilayer screens may be evaluated from the following equation obtained by substitution of Eq.(11) into Eq.(13):

$$\varepsilon=1-\pi dS_m N/\{4\omega(1+\alpha)\}. \quad (14)$$

Terefore, in the following correlation of the experimental data, the porosities ε for multilayer screens were calculated from Eq.(14). When, as shown by Ikeda[7], the hydraulic diameter d_h is defined as the

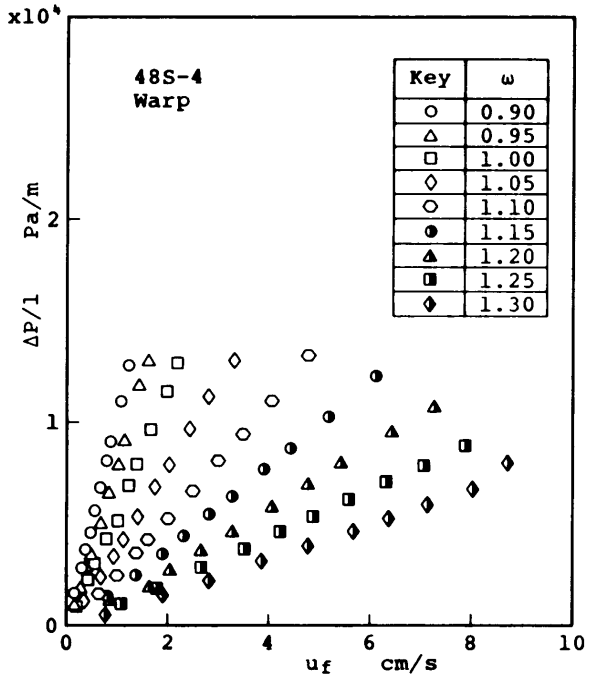

Fig. 4 Influence of packing number on pressure drop

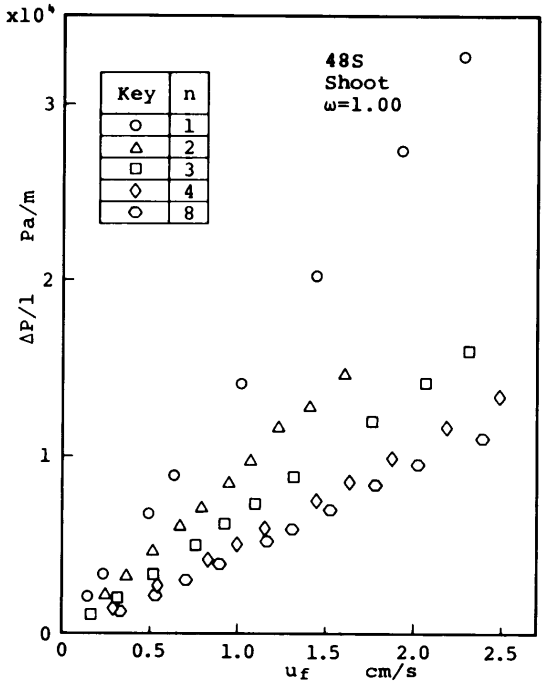

Fig. 5 Influence of number of screen layers on pressure drop

porous channel volume divided by the wetted area considered to be the sum of the surface area of the screen wires and inside surface area of the flow channel, the following expressions are obtained :

$$d_h=\varepsilon d/\{(1-\varepsilon)Z\} \quad (15)$$

$$Z=1+(1/n+\omega/\beta)/(\pi d S_m N), \quad (16)$$

where $\beta=b/\delta_1$ and b is the channel width. Thus, using Eq.(15), the friction factor C_f and the Reynolds number Re are expressed by the following equations :

$$C_f=\frac{\Delta P d_h}{2l\rho_l u^2}=\frac{\Delta P d\varepsilon^3}{2l\rho_l u_f^2(1-\varepsilon)Z} \quad (17)$$

$$Re=\frac{ud_h}{\nu_l}=\frac{du_f}{\nu_l(1-\varepsilon)Z}. \quad (18)$$

The experimental data obtained for various packing number ω using the screen samples of 200S-16 were correlated in the relation between C_f and Re, and the results are shown in Fig. 6. In this figure, the data fall on a separate line for each ω and shift downward as ω becomes large. The same result was obtained for almost all of the screen samples. This seems to be caused by the influence of the gap between the screen layers. As seen from Fig. 6, the experimental data nearly fall on the straight line with the gradient of almost minus unity for all ω. Therefore, the friction factor C_f can be expressed by the following expression :

$$C_f=A/Re. \quad (19)$$

The values of the coefficient A were determined from the experimental data for various ω of each screen sample using the least squares method. The relation between the coefficient A and the packing number ω is shown in Fig. 7. The scatter of the data is considerably small for $0.90\leqq\omega\leqq1.00$, but becomes large for $\omega>1.00$. Around $\omega=1.05$, the experimental data generally indicate the stepwise change in the value of A and some data show the change in the gradient. This is because the liquid tends to flow through larger gaps between screen layers rather than through the inside pore of the screens and because the additional channel between the channel walls and the screens is formed due to the curvature of screens. The rectangular screen generally has the peculiarity of curving in the direction of the short sides when it is left free. As the relation between A and ω, the following equation is derived from the data for $0.90\leqq\omega\leqq1.00$:

$$A=408\exp(-2.94\omega). \quad (20)$$

The solid line indicated in Fig. 7 is Eq.(20). Figures 8 (a)~8(c) show the relation between the friction factor C_f and the Reynolds number Re for the packing numbers of 0.90, 0.95, and 1.00, respectively. Also, Fig. 9 shows the experimental results obtained for different number of screen layers using 48 and 100 mesh stainless steel screens. In Figs. 8 and 9, the solid lines indicate Eq.(19) into which Eq.(20) was substituted. From these figures, it can be seen that, although some experimental values, e.g. the data for 200S-16, are slightly greater than the calculated ones, Eq.(20) satisfactorily correlates the experimental data for $0.90\leqq\omega\leqq1.00$, regardless of the mesh number, the number of screen layers and the flow direction through the mesh screens. Figure 10 shows the result obtained from the unsteady flow experiment[8]. These data were obtained for $0.70\leqq\omega\leqq0.82$, which is beyond

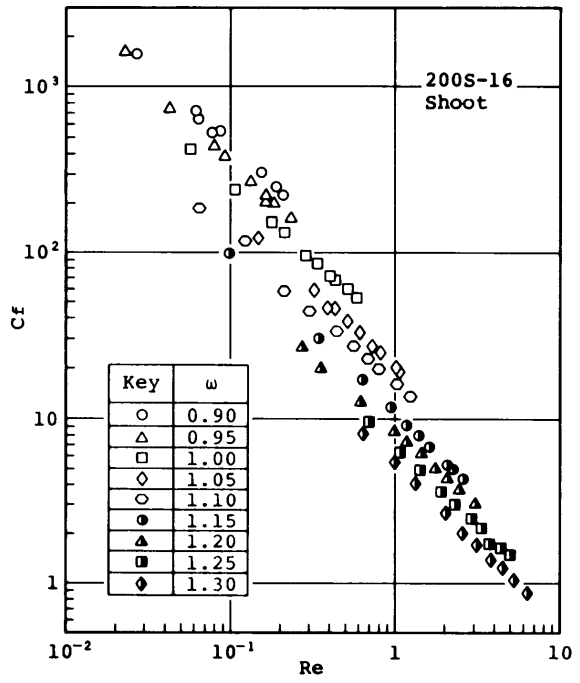

Fig. 6 Influence of packing number on relation between friction factor and Reynolds number

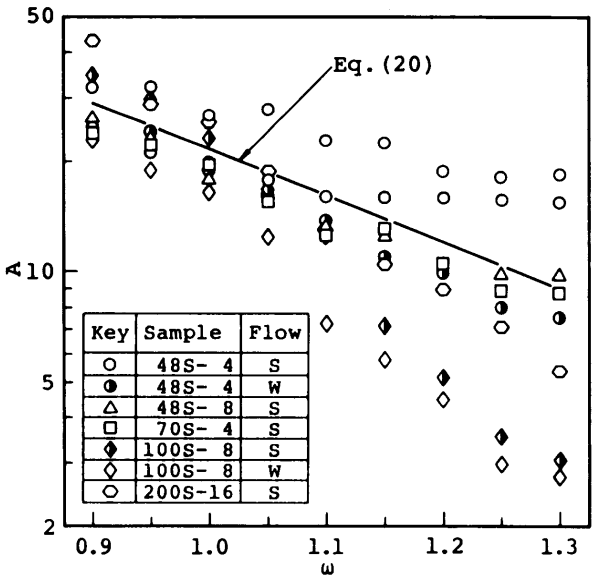

Fig. 7 Relation between coefficient A in Eq.(19) and packing number

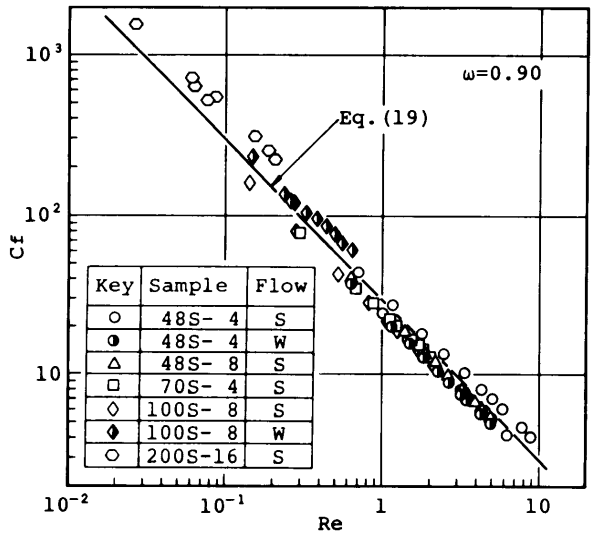

(a) $\omega=0.90$

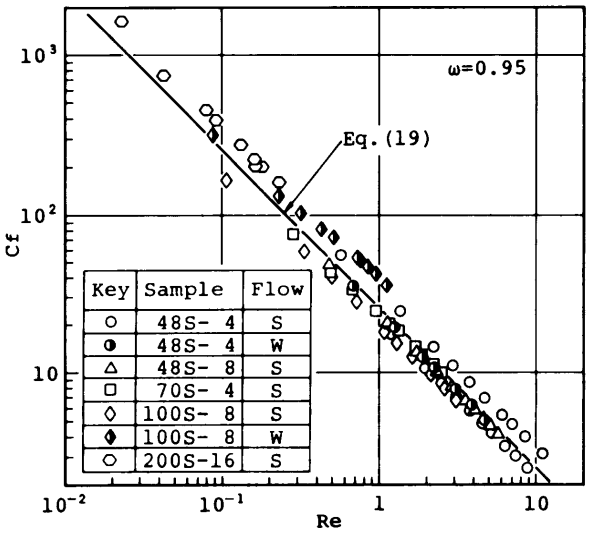

(b) $\omega=0.95$

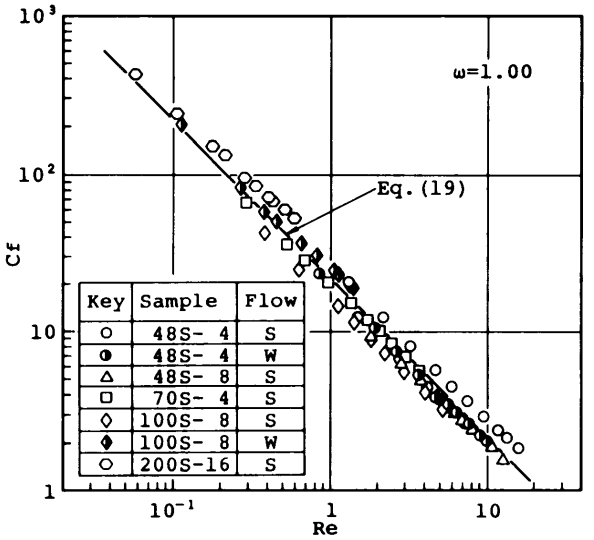

(c) $\omega=1.00$

Fig. 8 Relation between friction factor and Reynolds number

the present experimental conditions. As seen from Fig. 7, the slopes of the data seem to become smaller in the vicinity of $\omega=0.90$. Also, it seems that for $\omega \leqq 0.90$, the coefficient A approaches a constant value with decreasing ω. This is because the screen wicks can be considered as homogeneous porous materials when the gap between screen layers decreased. Thus, the following equation obtained by substitution of $\omega=0.90$ into Eq.(20) is shown by the solid line in Fig. 10 :

$$C_f=28.9/Re. \quad (21)$$

Since the data from the unsteady flow experiment can be correlated well with Eq.(21), Eq.(21) is thought to be valid for prediction of the friction factor C_f for $\omega<0.90$. For $\omega \leqq 0.90$, therefore, the screen wicks can be considered as homogeneous porous materials. In Fig.

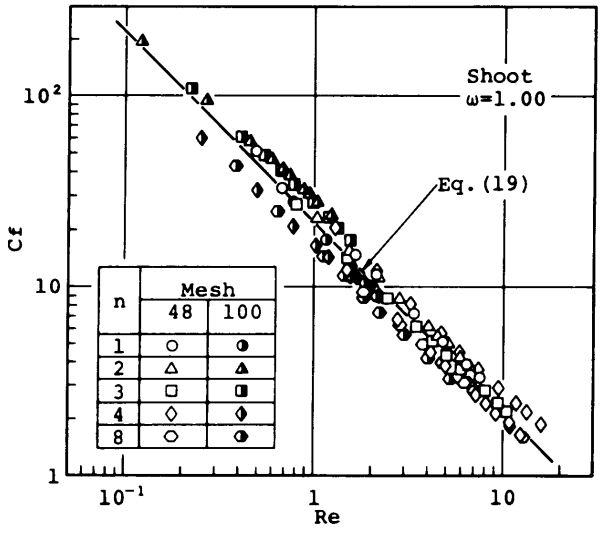

Fig. 9 Influence of number of screen layers on friction factor

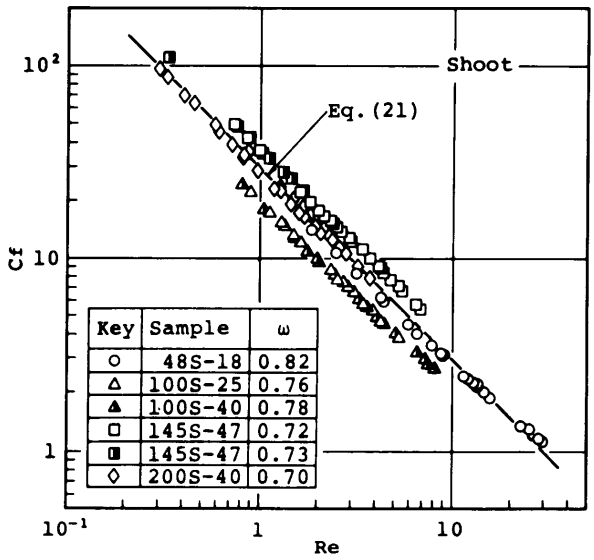

Fig. 10 Correlation of pressure drop data obtained from unsteady flow experiment

10, the data for 100 mesh stainless steel screens are slightly smaller than Eq.(21). This is because the values ε calculated from Eq.(14) are about 8% smaller than those obtained from Eq.(13) using the experimental values of ε_1.

The permeability K is expressed by Eq.(22) derived from Darcy's law :

$$K=\nu_l\rho_l l u_f/\Delta P. \quad (22)$$

The combination of Eqs.(17), (18), (19) and (22) yields the following equation :

$$K=d^2\varepsilon^3/\{2A(1-\varepsilon)^3)^2Z^2\} \quad (23)$$

Figure 11 shows the relation between the permeability K and the packing number ω. In Fig. 11, the equations for the permeability proposed by other investigators are also indicated. The permeability increases with the increase in ω, and in the case of 200S-16, the experimental values for $\omega=1.30$ are 25 times as large as those for $\omega=0.90$. Also, the experimental values are in good agreement with Eq.(23) into which Eq.(20) was substituted for A. On the contrary, the modified Blake - Kozeny equation [4]~[6] is in close agreement with the experimental values near $\omega=0.90$, but generally gives smaller values. Also, the equations by Ikeda[7] and by the unsteady flow experiment[8] agree with the experimental values only around $\omega=1.00$. Figure 12 shows the influence of the number of screen layers on the permeability. The solid lines shown in Fig. 12 are Eq.(23), into which Eq.(20) was substituted. As seen from Fig.12, the permeability increases with the increase in the number of screen layers, and for $\omega=1.00$, the calculated values are in close agreement with the experimental ones. However, for $\omega=1.20$, the agreement between the calculated and experimental values is not sufficient when the number of screen layer decreases. This seems to be because, for the same packing number, the gap between screen layers and the degree of the screen curvature are different by the number of screen layers.

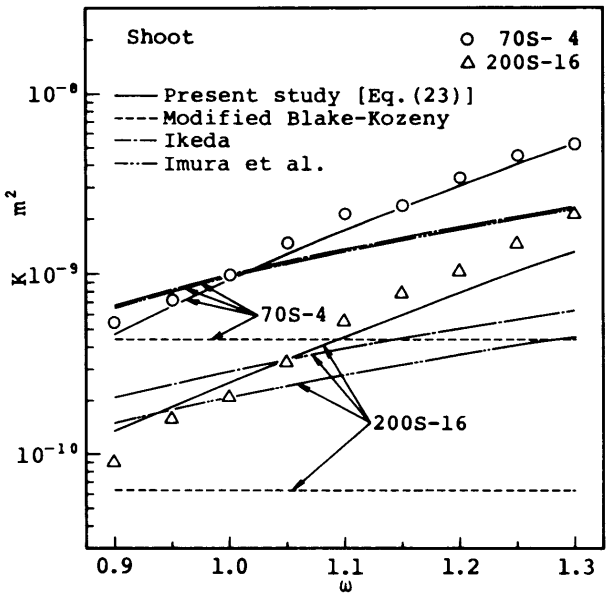

Fig. 11 Relation between permeability and packing number

6. Conclusions

The experimental study was performed on the permeability of screen wicks, and the effects of screen mesh size, number of screen layers and hold-down pressure were examined. Also, the equation for the permeability was presented based on the model of the screen geometry. The results drawn by this study are as follows :

(1) The porosity ε_1 for the single-layer screens can be predicted from Eq.(11) derived by the screen geometric model.

(2) The friction factor C_f of the screen wicks may be correlated by the expression $C_f=A/Re$ when Eq.(14) was used for porosity. The value of A for $\omega \geqq 0.90$ decreases with the increase in ω because of the increase of the gap between screen layers. For $0.90 \leqq \omega \leqq 1.00$, the coefficient A is represented with Eq.(20), and the friction factor can be correlated well with Eq. (19), into which Eq.(20) was substituted. For $\omega<0.90$, the friction factor C_f can be predicted from Eq.(21).

(3) The permeability for the screen wicks varies greatly with the hold-down pressure of screens, i.e., the packing number ω, and becomes large with the increase in the number of screen layers. For $\omega \leqq 1.00$, the permeability can be predicted from Eq.(23) using Eqs.(20) and (21). However, for $\omega>1.00$, the scatter of the data is large due to the difference of the screen installation. Therefore, in this case, the accurate esti-

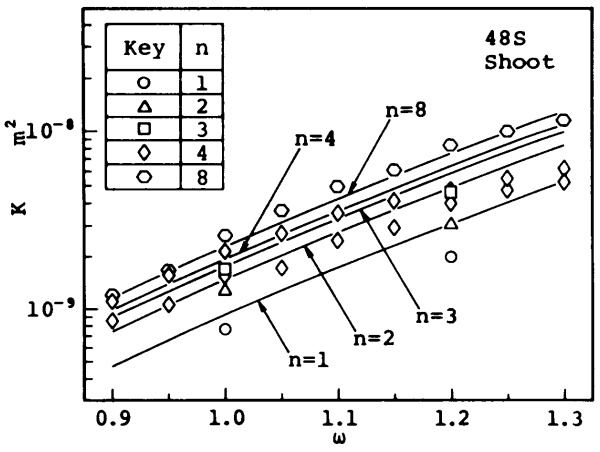

Fig. 12 Influence of number of screen layers on permeability (comparison between Eq. (23) and experimental values)

mation of the permeability is difficult.

Acknowledgments

The authors wish to thank Mr. M. Fujii and Mr. T. Maeda for their assistance in performing the experiment, and Mr. Y. Tachiyama for his cooperation in making the experimental setup.

References

(1) Kozai, H., Imura, H. and Ikeda, Y., The Effective Pore Radius of Screen Wicks, Trans. Jpn. Soc. Mech. Eng., (in Japanese), Vol. 56, No. 521, B (1990), p. 168.

(2) Kunz, H.R., Langston, L.S., Hilton, B.H., Wyde, S. S. and Nashick, G.H., Vapor-Chamber Fin Studies (Transport Properties and Boiling Characteristics of Wicks), NASA CR-812, (1967), p. 93.

(3) Phillips,E.C., Low - Temperature Heat Pipe Research Program, NASA CR-66792, (1969), p.25.

(4) Marcus, B.D., Theory and Design of Variable Conductance Heat Pipes, NASA CR-2018, (1972), p. 49.

(5) Chi, S.W., Heat Pipe Theory and Practice, (1976), p. 41, McGraw-Hill.

(6) Oshima, K., Matsushita, T. and Murakami, M., Heat Pipe Engineering, (in Japanese), (1979), p. 124, Asakura Shoten.

(7) Ikeda, Y., The Permeability of a Screen Wick, Trans. Jpn. Soc. Mech. Eng., (in Japanese), Vol. 52, No. 479, B(1986), p. 2612.

(8) Imura, H., Kozai, H., Hayashida, S. and Takashima, K., Heat-Transfer Characteristics in Screen-Wick Heat Pipes, JSME Int. J., Ser.II , Vol. 31, No. 1(1988), p. 88.